



Cite this: *RSC Adv.*, 2024, **14**, 31409

## Synthesis, *in vitro* biological evaluation and *in silico* studies of novel pyrrolidine derived thiosemicarbazones as dihydrofolate reductase inhibitors<sup>†</sup>

Hina Aftab,<sup>a</sup> Saeed Ullah,<sup>b</sup> Ajmal Khan,<sup>bc</sup> Mariya al-Rashida,<sup>d</sup> Talha Islam,<sup>d</sup> Abdulrahman Alshammari,<sup>e</sup> Norah A. Albekairi,<sup>e</sup> Parham Taslimi,<sup>id</sup> Ahmed Al-Harrasi,<sup>\*b</sup> Zahid Shafiq<sup>id</sup> <sup>\*a</sup> and Saeed Alghamdi<sup>g</sup>

Dihydrofolate reductase (DHFR) is a crucial enzyme involved in folate metabolism and serves as a prime target for anticancer and antimicrobial therapies. In this study, a series of 4-pyrrolidine-based thiosemicarbazones were synthesized and evaluated for their DHFR inhibitory activity. The synthesis involved a multistep procedure starting from readily available starting materials, leading to the formation of diverse thiosemicarbazone 5(a–r) derivatives. These compounds were then subjected to *in vitro* assays to evaluate their inhibitory potential against DHFR enzyme. The synthesized compounds 5(a–r) exhibited potent inhibition with IC<sub>50</sub> values in the range of 12.37 ± 0.48 μM to 54.10 ± 0.72 μM. Among all the derivatives 5d displayed highest inhibitory activity. Furthermore, molecular docking and ADME studies were performed to understand the binding interactions between the synthesized compounds and the active site of DHFR. The *in vitro* and *in silico* data were correlated to identify compounds with promising inhibitory activity and favorable binding modes. This comprehensive study provides insights into the structure–activity relationships of 4-pyrrolidine-based thiosemicarbazones as DHFR inhibitors, offering potential candidates for further optimization towards the development of novel therapeutic agents.

Received 13th July 2024  
 Accepted 25th September 2024  
 DOI: 10.1039/d4ra05071a  
[rsc.li/rsc-advances](http://rsc.li/rsc-advances)

## 1. Introduction

Folate metabolism has emerged as a promising and significant target for the creation of anti-cancer, anti-bacterial, and anti-parasitic therapeutic medicines in the last several years.<sup>1</sup> Dihydrofolate reductase (DHFR) plays a crucial role in reducing 7,8-dihydrofolate (DHF) to 5,6,7,8-tetrahydrofolate (THF) in cooperation with NADPH.<sup>2</sup> The production of thymidine (a precursor for DNA replication), purine nucleotides, glycine, methionine,

serine, and *N*-formyl-methionyl tRNA all rely on this chemical as a precursor to the cofactors needed for these reactions.<sup>3</sup> Cell development is restricted due to partial depletion of intracellular reduced folates caused by DHFR inhibition.<sup>4</sup> Antibacterial DHFR inhibitors work by preventing the production of DNA, RNA, and proteins, which in turn stops the proliferation of cells. Consequently, DHFR becomes a prime target for anticancer and anti-bacterial drugs. A decrease in DHFR enzyme activity lowers the intracellular THF pool, which impacts the concentration of folate coenzymes and, by extension, the production of purines and pyrimidines.<sup>5,6</sup> Since methyl-THF is required for homocysteine remethylation to produce methionine, an essential component of *S*-adenosylmethionine (SAM) required for the majority of biological methylation reactions, this may also affect homocysteine levels and methylation processes. Higher eukaryotic cells must rely on exogenous folic acid because, unlike prokaryotes and lower eukaryotic cells, they are unable to produce folates *de novo*. So, to acquire medications to treat infectious disorders caused by protozoan parasites and bacteria, the folic acid production route is an easy target.<sup>7</sup> Several DHFR inhibitors, as separate entities, have found clinical utility as antitumor agents.<sup>8–10</sup> One of the most potent DHFR inhibitor methotrexate (MTX) is one the first chemotherapeutic agent discovered and is still a support in single agent and combination cancer chemotherapy.<sup>11</sup>

<sup>a</sup>Institute of Chemical Sciences, Bahauddin Zakariya University, Multan-60800, Pakistan. E-mail: zahidshafiq@bzu.edu.pk

<sup>b</sup>Natural and Medical Sciences Research Centre, University of Nizwa, P.O. Box 33, PC 616, Birkat Al Mauz, Nizwa, Sultanate of Oman. E-mail: aharrasi@unizwa.edu.om

<sup>c</sup>Department of Chemical and Biological Engineering, College of Engineering, Korea University, 145 Anam-ro, Seongbuk-gu, Seoul 02841, Republic of Korea

<sup>d</sup>Department of Chemistry, Forman Christian College (A Chartered University) Lahore, Pakistan

<sup>e</sup>Department of Pharmacology and Toxicology, College of Pharmacy, King Saud University, Post box 2455, Riyadh, 11451, Saudi Arabia

<sup>f</sup>Department of Biotechnology, Faculty of Science, Bartin University, 74100 Bartin, Turkey

<sup>g</sup>Department of Pharmacy, Riyadh Security Forces Hospital, Ministry of Interior, Kingdom of Saudi Arabia

† Electronic supplementary information (ESI) available. See DOI: <https://doi.org/10.1039/d4ra05071a>



One of the nitrogen heterocycles utilized extensively by medicinal chemists to derive molecules for the treatment of human diseases is the five-membered pyrrolidine ring. This saturated scaffold is of great interest for three reasons: (1) the ability to efficiently explore the pharmacophore space *via*  $sp^3$ -hybridization; (2) the impact on the molecule's stereochemistry; and (3) the increased three-dimensional (3D) coverage caused by the ring's non-planarity; a phenomenon known as "pseudo rotation".<sup>12</sup> Additionally, the nitrogen atom of pyrrolidine ring has the capability to engage in hydrogen bonding interactions with amino acids residues present within active site of DHFR, thereby enhancing the compound's binding affinity. Its size and shape are well-suited for fitting into the active site pocket of DHFR. This facilitates favorable van der Waals interactions with nearby amino acids residues, which in turn enhances the stability of the enzyme–inhibitor complex.<sup>13</sup> The incorporation of heteroatomic fragments into the molecules is a thoughtful decision, as they serve as valuable tools for adjusting physicochemical parameters and achieving optimal ADME outcomes for potential drug candidates.<sup>14,15</sup>

Thiosemicarbazones are a fascinating class of compounds. Numerous pharmacological and biological features have been discovered including their efficacy as anti-urease,<sup>16,17</sup> chemosensing,<sup>18</sup> antibacterial,<sup>19</sup> antifungal,<sup>20</sup> anticancer,<sup>21</sup> anti-folate,<sup>22,23</sup> antidiabetic activity<sup>24</sup> and antimicrobial activity.<sup>25</sup> On the other hand, thiosemicarbazones also belong to one of the main families of DHFR (dihydrofolate reductase) inhibitors<sup>26,27</sup> due to the formation of stable complexes with zinc ions present in the active side of DHFR.<sup>28,29</sup> As thiosemicarbazones are known as chelate metal ions, this chelation helps in binding and inhibiting the enzyme. Furthermore, thiosemicarbazones possess a thioamide ( $-\text{CSNH}-$ ) functional group, which may also participate in hydrogen bonding interactions with specific amino acids residues in the DHFR active site, these interactions helps to stabilize the inhibitor in the enzyme's binding pocket, enhancing its potency.<sup>28,30</sup> The structural characteristics and redox activities of thiosemicarbazones contribute to their efficacy as anticancer agents, making them promising candidates for further exploration as DHFR inhibitors.<sup>31</sup>

Molecular hybridization involves merging different molecules to create new compounds. In our study, we synthesized novel 4-pyrrolidine based thiosemicarbazones by combining 4-pyrrolidinyl-benzaldehyde with thiosemicarbazide derivatives. These compounds were then evaluated for their effectiveness against the enzyme DHFR. Additionally, we conducted molecular docking, ADMET studies, and explored structure-activity relationships to understand the properties and potential of these compounds as DHFR inhibitors.

Structures of some pyrrolidine and thiosemicarbazones based dihydrofolate reductase (DHFR) inhibitors reported in literature are shown in (Fig. 1).<sup>32–35</sup>

## 2. Results and discussion

### 2.1 Chemistry

Pyrrolidine and thiosemicarbazone moieties have a wide range of biological and pharmacological effects. Therefore, it is

reasonable to integrate these two components into a unified molecular framework to create more potent biologically active compounds, such as those depicted in Fig. 1. The desired compounds were synthesized by modifying pyrrolidine moiety through the introduction of 4-fluorobenzaldehyde. This modification primarily involves replacing the NH group of pyrrolidines with 4-fluorobenzaldehyde instead of the hydrogen atom at the N–H position of pyrrolidine, and forming thiosemicarbazones by reacting with thiosemicarbazides, thus enhancing their biological activity. The targeted compounds **5(a–r)** were prepared by the substitution at N–H position which was done by the reaction of pyrrolidine (**1**) with 4-fluorobenzaldehyde (**2**) using anhydrous  $\text{K}_2\text{CO}_3$  and DMF at 90 °C for 12 h, giving 4-(pyrrolidin-1-yl)benzaldehyde (**3**). The synthesis of thiosemicarbazones was achieved by reaction of compound (**3**) with thiosemicarbazides **4(a–r)**. The synthetic route in synthesis of 4-pyrrolidine based thiosemicarbazones **5(a–r)** was displayed in Scheme 1.

The structure of synthesized compounds was confirmed using various advanced spectroscopic techniques. In the  $^1\text{H}$ -NMR spectra of the pyrrolidine-based thiosemicarbazones, a prominent single peak appeared within the chemical shift range of  $\delta$  11.9–10.1 ppm, revealing of NH-protons presence. Furthermore, the protons of  $\text{N}=\text{CH}$  were prominent between  $\delta$  7.95 and 9.13 ppm. Notably, C–H protons in the benzene moiety exhibited distinct signals within the range of  $\delta$  7.0–8.0 ppm, while those in the pyrrolidine group were identified within  $\delta$  1.0–5.0 ppm. Furthermore, negative signals observed in  $^{13}\text{C}$ -NMR spectra suggested the presence of  $\text{CH}_2$  groups in the compounds. Other characteristic signals were detected at  $\delta$  23.5, 33.9, 175.8 ppm, corresponding to  $\text{CH}_3$  and  $\text{CH}$ , as well as  $\text{C}=\text{S}$  functionalities. In order to determine the purity of compounds, HPLC analysis was carried out using  $\text{CH}_3\text{CN} : \text{H}_2\text{O} = 80 : 20$  eluent system with 263 nm wavelength. All the compounds exhibited great than 95% purity.

### 2.2 Pharmacology

**2.2.1 Biological activity.** The inhibitory activity of synthesized compounds was evaluated against the dihydrofolate reductase enzyme, utilizing methotrexate as a positive control with an  $\text{IC}_{50}$  value of  $0.086 \pm 0.07 \mu\text{M}$ . The inhibitory activity data, represented as  $\text{IC}_{50}$  values, is presented in Table 1. The results indicated that the target compounds displayed  $\text{IC}_{50}$  in the range of  $12.37 \pm 0.48 \mu\text{M}$  to  $54.10 \pm 0.72 \mu\text{M}$ . Among all derivatives, **5d** and **5l** exhibited highest inhibition activity with  $\text{IC}_{50}$  value  $12.37 \pm 0.48$  and  $12.38 \pm 0.25 \mu\text{M}$ . Among the compounds, **5d**, **5e**, **5f**, **5g**, **5l** and **5m** exhibited good inhibitory potential with  $\text{IC}_{50}$  values in the range of  $12.38 \pm 0.25 \mu\text{M}$  to  $21.18 \pm 0.44 \mu\text{M}$ . Derivative **5l** exhibited the highest inhibitory activity against dihydrofolate reductase enzyme with  $\text{IC}_{50} = 12.38 \pm 0.25 \mu\text{M}$ , followed by **5d** with  $\text{IC}_{50} = 12.37 \pm 0.48 \mu\text{M}$ , **5e** ( $\text{IC}_{50} = 15.30 \pm 0.26 \mu\text{M}$ ), **5f** ( $\text{IC}_{50} = 21.18 \pm 0.44 \mu\text{M}$ ), **5g** ( $\text{IC}_{50} = 14.37 \pm 0.29 \mu\text{M}$ ) and **5m** ( $\text{IC}_{50} = 16.27 \pm 0.26 \mu\text{M}$ ). Compound **5a**, **5h**, **5i**, and **5n** showed moderate inhibition potency compared to the standard with  $\text{IC}_{50}$  ranging from  $22.06 \pm 0.37 \mu\text{M}$  to  $29.11 \pm 0.38 \mu\text{M}$ . Compounds **5b**, **5c**, **5j**, **5k**, **5o**, **5p**, **5q** and



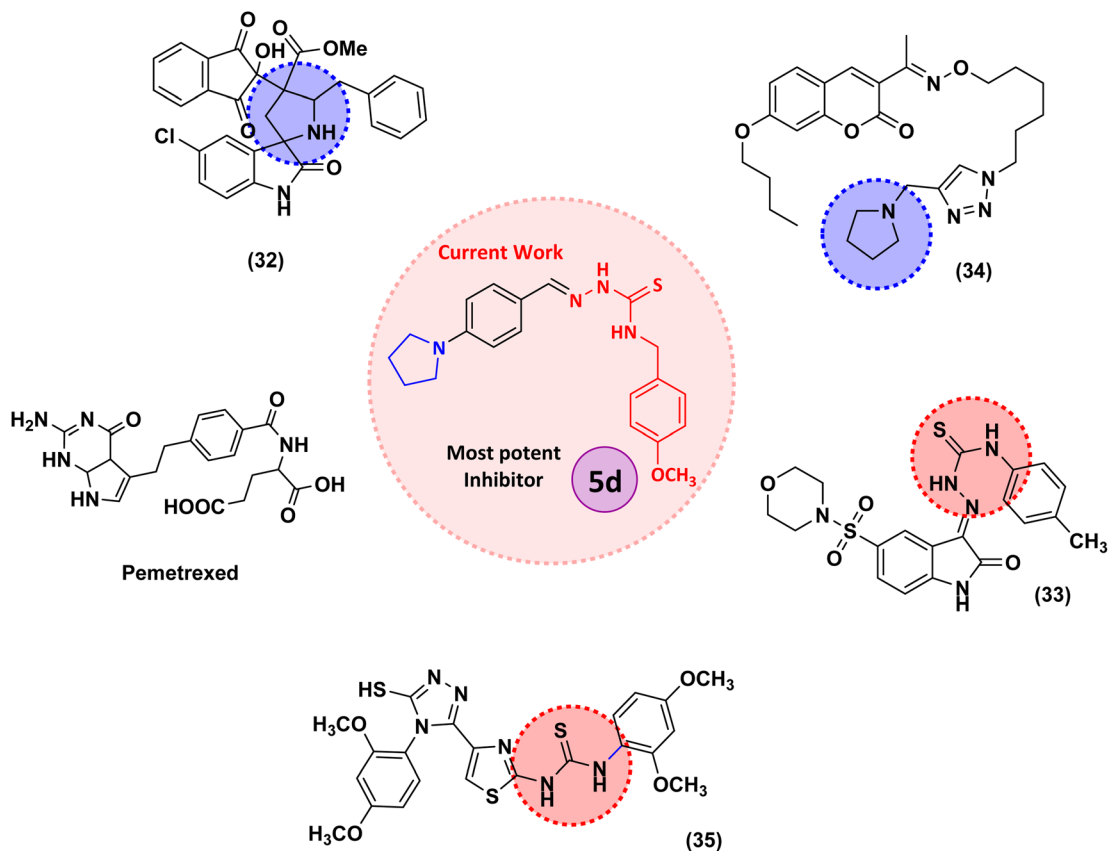


Fig. 1 Reported pyrrolidine and thiosemicarbazone based DHFR Inhibitors.

**5r** showed moderate to least inhibition activity compared to methotrexate with  $IC_{50}$  value as follows.

**5b**  $33.10 \pm 0.71$

**5c**  $36.20 \pm 0.69$

structure–activity link. The inhibitory potential of thiosemicarbazone is explored by changing the R group on the

**5o**  $45.28 \pm 0.63$

**5p**  $48.15 \pm 0.60$

**5j**  $54.10 \pm 0.72$

**5q**  $35.26 \pm 0.59$

**5k**  $40.62 \pm 0.59$

**5r**  $42.16 \pm 0.63$

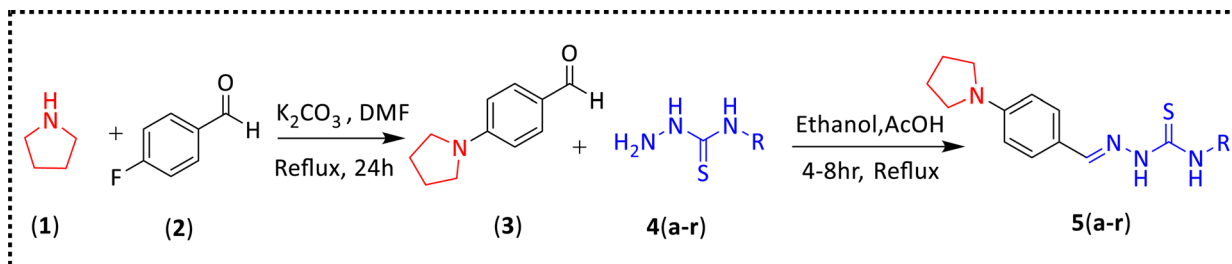
Compound **5j** was the least potent member of the series with  $IC_{50}$  value of  $54.10 \pm 0.72 \mu\text{M}$ .

### 2.3 Structure–activity relationship

Thiosemicarbazones exhibit the remarkable ability to hinder the activity of the DHFR enzyme, thereby disrupting folate metabolism pathways crucial for DNA synthesis and cellular proliferation. This exceptional characteristic renders thiosemicarbazones promising candidates for anti-cancer and anti-microbial therapies. A novel series of thiosemicarbazones, based on 4-pyrrolidinyl-benzaldehyde, has been synthesized and assessed for their efficacy against the dihydrofolate reductase enzyme. The  $IC_{50}$  values and percentage inhibition of these synthesized compounds were determined and is presented in Table 1. Thiosemicarbazone and 4-pyrrolidinylbenzaldehyde functioned as significant structural frameworks, and the phenyl or benzyl group bonded to the  $N^4$  nitrogen of thiosemicarbazone was crucial in establishing an indisputable

thiosemicarbazides moiety. The R group is varied with aromatic, non-aromatic and aliphatic groups. The compounds **5f** and **5p** with phenyl and benzyl rings respectively, by comparison, phenyl derivative has more inhibition potential than benzyl derivative. In case of compound **5l** and **5d** with phenethyl and 4-methoxyphenyl moieties showed maximum inhibition potencies. Compounds **5j** and **5o** with para and meta-nitro group on the phenyl ring, among them meta-substitution is slightly active (**5o**,  $IC_{50} = 45.28 \pm 0.63 \mu\text{M}$ ) as compared to para substitution (**5j**,  $IC_{50} = 54.10 \pm 0.72 \mu\text{M}$ ). Compounds **5d** and **5h** containing methoxy substitution at the para and meta positions of the phenyl ring respectively, **5d** showed much better inhibitory potency with  $IC_{50}$  value  $12.37 \pm 0.48 \mu\text{M}$  of than **5h** with  $IC_{50}$  value of  $23.11 \pm 0.35 \mu\text{M}$ . Electron donating substituents, like alkyl groups, have the ability to increase the electron density around the benzene ring through resonance effects. This amplified electron density raises stronger interactions between the inhibitor molecule and the enzymes active





	<b>R</b>	<b>Yield (%)</b>	<b>Time, temperature</b>		<b>R</b>	<b>Yield (%)</b>	<b>Time, temperature</b>
<b>5a</b>	Cyclohexyl	75	5 h, 70 °C	<b>5j</b>	4-Nitrophenyl	85	4 h, 80 °C
<b>5b</b>	4-Fluorophenyl	81	7 h, 80 °C	<b>5k</b>	4-Ethylmorpholine	89	5 h, 70 °C
<b>5c</b>	2,3-Dichlorophenyl	91	8 h, 80 °C	<b>5l</b>	$\beta$ -Phenethyl	91	5 h, 70 °C
<b>5d</b>	4-Methoxyphenyl	87	5 h, 70 °C	<b>5m</b>	4-Bromophenyl	91	7 h, 80 °C
<b>5e</b>	2,6-Dimethylphenyl	85	8 h, 80 °C	<b>5n</b>	3-Bromophenyl	85	7 h, 80 °C
<b>5f</b>	Phenyl	83	5 h, 70 °C	<b>5o</b>	3-Nitrophenyl	85	5 h, 80 °C
<b>5g</b>	4-Methylphenyl	81	5 h, 70 °C	<b>5p</b>	Benzyl	85	5 h, 70 °C
<b>5h</b>	3-Methoxyphenyl	95	5 h, 70 °C	<b>5q</b>	2-Fluorophenyl	87	8 h, 80 °C
<b>5i</b>	4-Chlorobenzyl	79	7 h, 80 °C	<b>5r</b>	4-Methylbenzyl	87	5 h, 70 °C

**3** = 5 mmol, **4(a-r)** = 5 mmol (1 : 1)

Scheme 1 Synthetic route for the preparation of thiosemicarbazones.

site, potentially leading to more potent inhibition. Moreover, the positive inductive effect (+I) exerted by alkyl groups on the benzene rings further intensifies its electron density. This phenomenon enhances the inhibitor's capacity to engage with the enzyme's active site. Therefore, with increase in alkyl substitution inhibition potential is increased as we see in compound **5e** when compared with **5g** and **5r**. In case of methyl substitutions at para position of phenyl and benzyl rings of compound **5g** and **5r** with  $IC_{50} = 14.37 \pm 0.29 \mu M$  and  $IC_{50} = 42.16 \pm 0.63 \mu M$  respectively, **5g** is more potent as compared to **5r**. The compound **5e** with dimethyl substitution ( $IC_{50} = 15.30 \pm 0.26 \mu M$ ) slightly increases inhibition potency than one methyl substitution. In case of halogens, with the increase in number of substitutions, potency is somewhat decreased, possibly due to electron-withdrawing effect. This effect makes

any carbon center even more electron-deficient than before also causes negative inductive effect (-I). Their activity order is Br > Cl > F. Compounds **5m** and **5n** with bromo substitution at para and meta positions of phenyl ring respectively, among them **5m** ( $IC_{50} = 16.27 \pm 0.26 \mu M$ ) is more potent than **5n** ( $IC_{50} = 22.06 \pm 0.37 \mu M$ ). Compounds **5c**, and **5i** with 2,3-dichlorophenyl and 4-chlorobenzyl exhibited moderate inhibition with  $IC_{50} = 36.20 \pm 0.69$ ,  $IC_{50} = 27.46 \pm 0.50$  respectively. While in case of cyclohexyl containing compound **5a** moderate activity against enzyme was observed ( $IC_{50} = 29.11 \pm 0.38 \mu M$ ).

The study reveals a clear correlation between the chemical structure of the compounds and their inhibitory potency, as showed in Fig. 2. Notably, compounds featuring para substitution of the phenyl ring exhibit heightened potency in the series. Among these, compounds **5d** and **5l**, distinguished by 4-



**Table 1** IC<sub>50</sub> values of the synthesized compounds against dihydrosfolate reductase

Compounds R		
	% inhibition (0.5 mM)	IC <sub>50</sub> ± μM (SEM)
5a	83.58	29.11 ± 0.38
5b	80.64	33.10 ± 0.71
5c	81.29	36.20 ± 0.69
5d	91.14	12.37 ± 0.48
5e	90.25	15.30 ± 0.26
5f	86.20	21.18 ± 0.44
5g	89.53	14.37 ± 0.29
5h	86.71	23.11 ± 0.35
5i	83.90	27.46 ± 0.50
		Standard

**Table 1 (Contd.)**

Compounds R		
	% inhibition (0.5 mM)	IC <sub>50</sub> ± μM (SEM)
5j	74.10	54.10 ± 0.72
5k	76.90	40.62 ± 0.59
5l	91.46	12.38 ± 0.25
5m	90.77	16.27 ± 0.26
5n	88.20	22.06 ± 0.37
5o	75.62	45.28 ± 0.63
5p	74.60	48.15 ± 0.60
5q	77.26	35.26 ± 0.59
5r	79.83	42.16 ± 0.63
Methotrexate	0.086 ± 0.07	

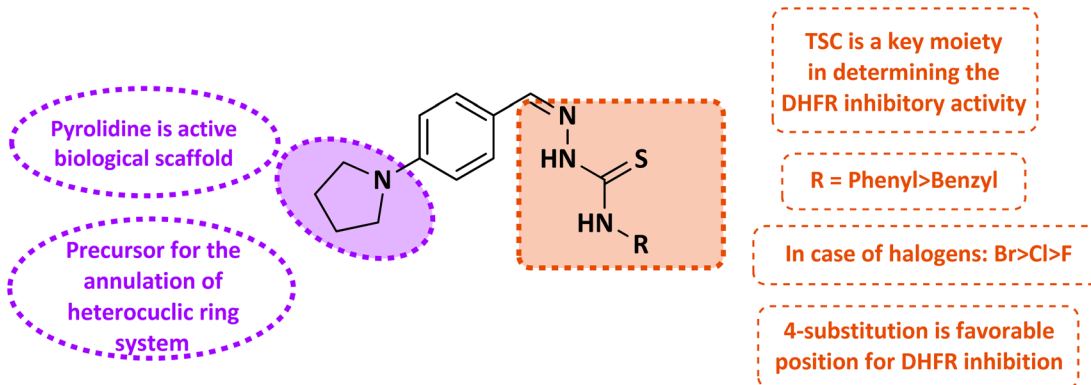


Fig. 2 Structure activity relationship of the synthesized thiosemicarbazones.

methoxyphenyl and phenethyl substitution, emerge as most potent in the series. Conversely, compound **5j**, with 4-nitrophenyl substitution, displays diminished activity. It becomes evident that the introduction of electron-withdrawing substituents on the phenyl ring leads to decreased inhibitory potential, whereas electron-donating substitutions enhance activity. This highlights the crucial role of understanding the electronic characteristics of substituents in modulating biological activity, thereby facilitating the rational design of more effective compounds.

#### 2.4 Molecular docking studies

The crystal structure of human dihydrofolate reductase (DHFR) in complex with the NADP and inhibitor SRI-9439 was downloaded from the PDB (PDB id: 1kms, 1.09 Å). To validate the docking protocol, the co-crystallized inhibitor was re-docked, the docking method was able to successfully reproduce the experimentally observed conformation for the ligand. The NADPH co-factor was retained for the docking studies in accordance with previous studies.<sup>36</sup> All compounds (**5a–r**) were docked and were found to bind in the same area of the active site as the co-crystallized inhibitor (Fig. 3). For reference, molecular docking of methotrexate was also carried out to map

out important interactions with the binding site amino acids. Details of binding site interactions are given in Table 2.

Compounds **5d**, the most active inhibitor of hDHFR was selected for in depth analysis of binding site interactions (Fig. 4). One of the NH groups was making a hydrogen bond with Ser59. Two carbon hydrogen bonds were observed between methoxy carbon and Val115 and Ile7, the same methoxy carbon was also making alkyl interactions with Val115 and NADP, and pi alkyl interaction with Phe34. The methoxy substituted phenyl ring was making pi alkyl contacts with the NADP and Leu22 and a pi-pi stacked contact with Leu34. While the other phenyl ring was making a pi-pi stacked interaction with Phe31.

#### 2.5 Molecular dynamics simulation studies

Analysis of protein–ligand RMSD show that the complex remained stable throughout the 100 ns simulation time period. The C $\alpha$  protein RMSD value remained between 1.0 Å to 2.3 Å during the whole simulation mostly around 2.0 Å during the last 50 ns of simulation (Fig. 5). In ligand fit on protein RMSD, the value varied during the first 25 ns up-to 8.0 Å, then remained stable between 5.0 Å to 6.0 Å and stabilized around 5.5 Å towards the end of simulation. In protein RMSF, C $\alpha$  protein all residues showed value less than 3.0 Å (Fig. 6). Protein secondary structure was % total SSE at 43.78, while  $\alpha$ -helix was 14.58 and  $\beta$ -strand at 29.21. Ligand RMSF values of fit ligand on protein showed all atoms have RMSF values between 2–3 Å where pyrrolidine moiety and methyl of anisole moiety showed relatively higher RMSF values as compared to other atoms in the ligand (ESI Fig. 1†). Protein–ligand contacts showed GLY 20 showed mostly hydrogen bonds and water bridges interactions with the highest interaction fraction around 0.6. Ligand–protein contacts showed nitrogen from thiosemicarbazide moiety formed interactions with GLY 20 for 55% of simulation time (ESI Fig. 2†). Ligand torsion profile showed most fluctuation and movement in the bonds of pyrrolidine and anisole moieties in the compound while thiosemicarbazide moiety remained relatively stable in bonds torsion (ESI Fig. 3†).

#### 2.6 ADME studies

*In silico* ADME evaluation of all compounds **5a–r** was carried out using Swiss ADME. Overall, all compounds indicated favorable



Fig. 3 Overlap of docked conformations of hDHFR inhibitors **5a–r**, NADPH is shown in black, the standard inhibitor drug methotrexate is shown in cyan color and the co-crystallized inhibitor is shown in blue.



Table 2 Binding site interactions of docked conformations of compounds (5a–r)

Code	Hydrogen bond	Distance (Å)	Hydrophobic			Other
			Alkyl	Pi-alkyl	Pi-pi stacked	
<b>5a</b>	SER59	1.74	ALA9	PHE34		
	ASP21	2.1	NDP202	LEU22		
	SER59	2.1		ILE60		
<b>5b</b>				NDP202		
	VAL115	1.9	PRO61	LEU22	PHE31	VAL8 halogen (fluorine)
	ASP21	2.67		PRO61	PHE34	GLU30 halogen (fluorine)
				ILE7		SER59 pi-lone pair
<b>5c</b>	PHE31	2.74	ILE60	PHE34	PHE31	
	PHE31	2.91	VAL115	LEU22		
<b>5d</b>	SER59	2.12	VAL115	PHE34	PHE31	
	ILE7	3.06	NDP202	LEU22	PHE34	
	VAL115	2.71		NDP202		
	NDP202	2.97				
<b>5e</b>	LEU22	2.43	PRO26	ILE60	PHE31	
	SER59	1.86	PRO61	PRO61		
	ASP21	1.74		PRO61		
	ASN64	3.03				
<b>5f</b>	SER59	2.14		LEU22	PHE31	
	PHE31	2.58		NDP202		
<b>5g</b>	SER59	2.15	ARG32	PHE34	PHE31	
			NDP202	LEU22	PHE34	
<b>5h</b>	VAL115	2.1	PRO26	PHE34	PHE31	
			PRO61	LEU22		
			ILE7	ILE60		
				PRO61		
				ALA9		
				NDP202		
	VAL115	2.03	ALA9		PHE31	
	ASN64	2.08	LEU22	TRP24	PHE34 (pi-pi T-shaped)	
<b>5i</b>	ASN64	1.79		TRP24		
				PHE31		
				PHE31		
				ALA9		
				LEU22		
				NDP202		
	THR136	2.31	PRO61	LEU22	PHE34	GLU30 attractive charge
	lig:H33 – VAL115:O	2.16		PRO61		SER59 pi-lone pair
<b>5j</b>	PHE34:HA:O25	2.96		ILE7		
				ALA9		
	ASP21	1.99	LEU67	ILE60		ASP21 salt bridge; attractive charge
	SER59	2.17				
	ASP21	3.01				
	SER59	1.94				
	ASP21	2.37				
	SER59	1.66		ILE60	PHE31	
<b>5l</b>	ASP21	1.64		PRO61		
				PRO26		
				PRO61		
	VAL115	1.9	ALA9	LEU22	PHE31	SER59 pi-lone pair
	ASP21	2.6	PRO61	PRO61	PHE34	
			ILE7			
			ALA9			
	SER59	1.76	LEU22	PHE31:Br24	PHE31	
<b>5n</b>	PHE31	2.33		ILE60	PHE34 (pi-pi T-shaped)	
				LEU22		
				NDP202		
	ASP21	1.94	VAL115	PHE34		
<b>5o</b>	VAL115	2.68	NDP202	LEU22		
	LEU22	3.17		ILE60		



Table 2 (Contd.)

Code	Hydrogen bond	Distance (Å)	Hydrophobic			
			Alkyl	Pi-alkyl	Pi-pi stacked	Other
<b>5p</b>	ASP21	1.94	VAL115 NDP202	PHE34 LEU22 PRO26	NDP202	
	VAL115	2.68			LEU22	
	LEU22	3.17			PRO26	
<b>5q</b>	SER59	1.73	ILE60 LEU22 PHE31	PHE31	ILE60 LEU22 PRO26	THR56 halogen (fluorine)
	ILE60	1.92				
	PHE31	2.85				
<b>5r</b>	PRO61	2.72	LEU67 ILE60	PHE34 ILE60 LEU22 ILE60	NDP202	

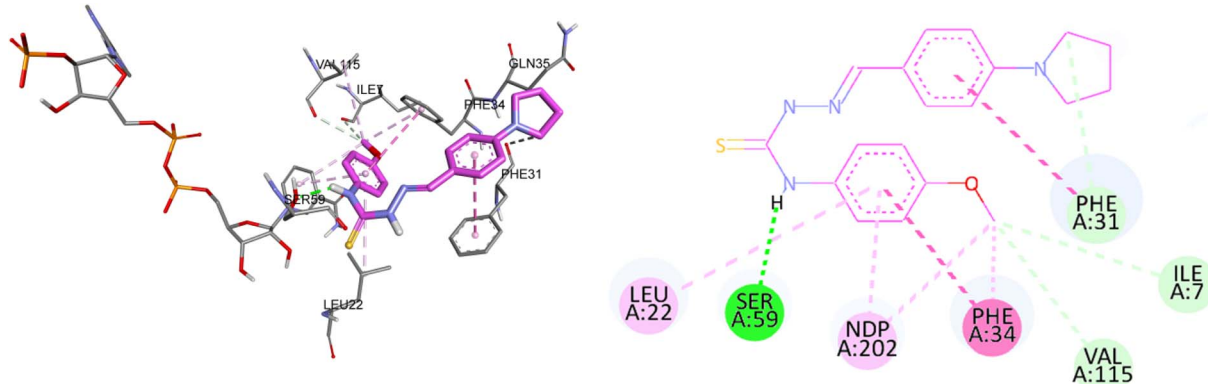


Fig. 4 3D and 2D binding site interactions of most hDHFR inhibitor 5d.

ADME profile as indicated by several physicochemical parameters given in (Table 3). Oral bioavailability of a compound is represented in the form of a bioavailability radar diagram based on parameters such lipophilicity, size, polarity, solubility, saturation rate and molecular flexibility. All compounds were predicted to have good oral bioavailability, as a selected example radar diagram of most active compound **5d** is shown in (Fig. 7). All compounds were predicted to have good to moderate water solubility, and with high gastrointestinal (GI) absorption. Interestingly most of the compounds were predicted to cross the blood-brain barrier (BBB). This ability to cross BBB, coupled with potent DHFR inhibition activity can be tailored for the design of novel anticancer drugs targeting brain tumors.

### 3. Experimental

#### 3.1 Chemistry

All of the chemicals needed to synthesize 4-(pyrrolidin-1-yl)benzaldehyde-based thiosemicarbazones were purchased from

Sigma-Aldrich. Petroleum ether, ethyl acetate, glacial acetic acid, ethanol, and methanol were among the chemicals and solvents purchased from Merck and utilized in their original forms. Aluminum-backed silica gel plates were used to monitor the start and finish of the reaction.  $^1\text{H}$  and  $^{13}\text{C}$ -NMR spectra of were obtained at 25 °C using a Bruker Ascend 600 MHz NMR spectrometer in deuterated solvent such as DMSO-d<sub>6</sub> (600 MHz for  $^1\text{H}$  and 151 MHz for  $^{13}\text{C}$ ). Chemical shifts (ppm) were used to portray NMR spectra, and coupling constants ( $\text{J}$ ) were shown in hertz (Hz) to show signal multiplicity HPLC was carried out on Agilent, Germany (liquid chromatographic column 150 mm × 4.6 mm (id) packed with 5-micron C18; 263 nm).

#### 3.2 General method for the synthesis of 4-(pyrrolidin-1-yl)benzaldehyde (3)

Compound (3) was synthesized using a method that had been previously reported.<sup>37</sup> To summarize, pyrrolidine (1 mmol) was dissolved in 4.0 ml of DMF. After that, the solution was heated



Ca (Lig) fit on Prot

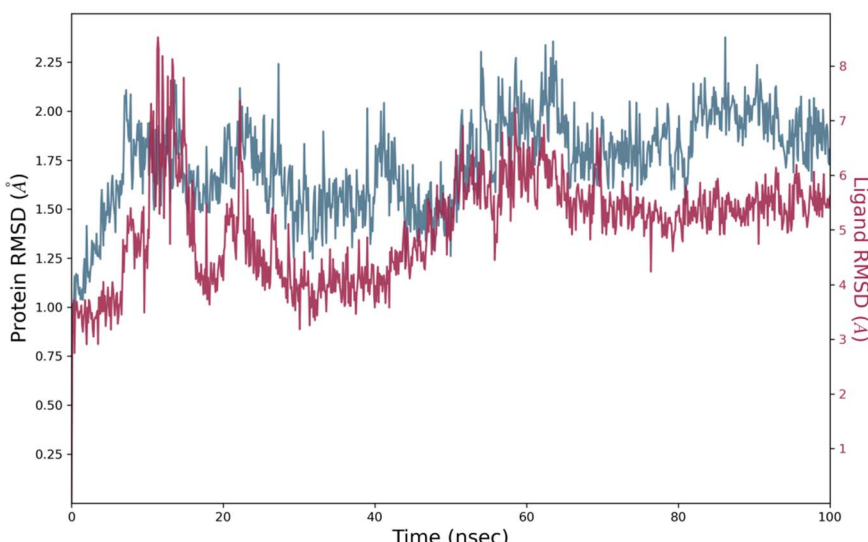


Fig. 5 RMSD graph of 5d-hDHFR protein ligand complex for 100 ns simulation run.

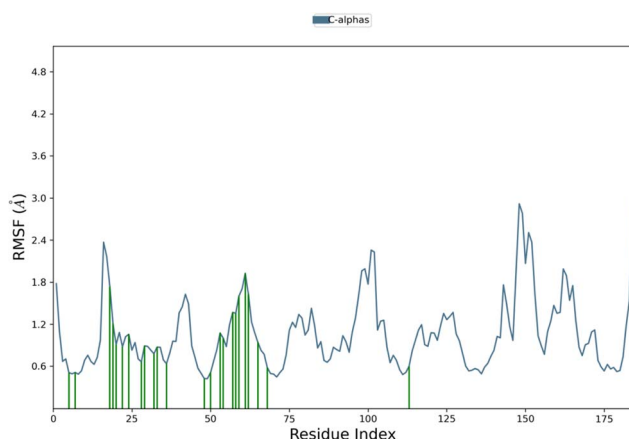


Fig. 6 Protein RMSF graph of 5d complexed with hDHFR. Residues that interact with the ligand are shown in green vertical bars.

to 80 °C, while being stirred, anhydrous K<sub>2</sub>CO<sub>3</sub> (2 mmol) was added. After 30 minutes, 4-fluorobenzaldehyde (1 mmol) was added in reaction mixture. The heating was continued for 12 hours. Once the reaction was finished, the mixture was cooled to room temperature and added to the ice water drop by drop. The product was precipitated out, filtered and dried. The formed product was pure and used without additional purification.

### 3.3 General method for the synthesis and characterization of compounds 5(a–r)

A previously reported<sup>38</sup> one-step condensation method was employed to synthesize thiosemicarbazones, with some modifications to the solvent, in a tropical setting. First, thiosemicarbazides (4a–r) (5 mmol) and compound (3) (0.1 g, 5 mmol) were mixed in a 20 ml ethanol solution in an oven-dried,

single-neck round bottom flask. As a catalyst, a small amount (three to four drops) of glacial acetic acid was added. After that, the mixture was refluxed for four to eight hours while thin layer chromatography (TLC) was used for monitoring the reaction's development. The resultant solid product was filtered and dried once the reaction was finished. The residue was then crystallized using ethanol to obtain the required thiosemicarbazones 5(a–r). Characterization data of each synthesized compound is given below.

**3.3.1 N-Cyclohexyl-2-[4-(pyrrolidin-1-yl)benzylidene]hydrazinecarbothioamide (5a).** Color: red, yield: 75%, melting point: 234–236 °C, δ<sub>H</sub> (600 MHz, DMSO-*d*<sub>6</sub>) 11.14 (1 H, s), 7.93 (1 H, s), 7.79 (1 H, d, *J* 8.6), 7.56 (2 H, d, *J* 8.3), 6.54 (2 H, d, *J* 8.4), 4.18 (1 H, ddt, *J* 11.2, 6.9, 3.8), 3.28 (4 H, d, *J* 6.3), 2.01–1.91 (4 H, m), 1.88 (2 H, dd, *J* 12.5, 4.2), 1.72 (2 H, dt, *J* 13.2, 3.7), 1.60 (1 H, dt, *J* 12.9, 3.9), 1.42 (2 H, qd, *J* 12.2, 3.5), 1.29 (2 H, qt, *J* 12.8, 3.4), 1.15 (1 H, ddd, *J* 15.9, 8.0, 3.5); <sup>13</sup>C NMR (151 MHz, DMSO) δ 175.37, 149.25, 143.91, 129.26, 121.07, 111.91, 52.77, 47.70, 32.45, 25.63, 25.42, 25.38, HPLC: CH<sub>3</sub>CN : H<sub>2</sub>O = 80 : 20; *t*R: 2.164 min, purity: 98.7%, C<sub>18</sub>H<sub>26</sub>N<sub>4</sub>S, QTOF MS ES<sup>+</sup> (*m/z*): [M + H]<sup>+</sup>, calcd: 331.1956, found: 331.1956.

**3.3.2 N-(4-Fluorophenyl)-2-[4-(pyrrolidin-1-yl)benzylidene]hydrazinecarbothioamide (5b).** Color: brown, yield: 81%, melting point: 249–251 °C, δ<sub>H</sub> (600 MHz, DMSO-*d*<sub>6</sub>) 11.59 (1 H, s), 9.92 (1 H, s), 8.03 (1 H, s), 7.68 (2 H, d, *J* 8.3), 7.58 (2 H, dd, *J* 8.7, 5.0), 7.19 (2 H, t, *J* 8.6), 6.55 (2 H, d, *J* 8.4), 3.28 (4 H, d, *J* 6.5), 1.97 (4 H, d, *J* 5.9); <sup>13</sup>C NMR (151 MHz, DMSO) δ 175.61, 160.74, 159.13, 149.41, 144.78, 136.08, 129.67, 128.27, 128.22, 120.94, 115.13, 114.98, 111.88, 47.71, 25.43, HPLC: CH<sub>3</sub>CN : H<sub>2</sub>O = 80 : 20; *t*R: 2.088 min, purity: 98.2%, C<sub>18</sub>H<sub>19</sub>FN<sub>4</sub>S, QTOF MS ES<sup>+</sup> (*m/z*): [M + H]<sup>+</sup>, calcd: 343.1392, found: 343.1392.

**3.3.3 N-(2,3-Dichlorophenyl)-2-[4-(pyrrolidin-1-yl)benzylidene]hydrazinecarbothioamide (5c).** Color: brown, yield: 91%, melting point: 301–303 °C, δ<sub>H</sub> (600 MHz, DMSO-*d*<sub>6</sub>) 11.85

Table 3 *In silico* ADME properties of compounds (5a–r)

Code	MW	RB	HBA	HBD	TPSA	log P	log S	GI	BBB	B score
5a	330.49	6	1	2	71.75	3.53	-4.60	High	Yes	0.55
5b	343.43	6	2	2	71.75	3.70	-5.95	High	No	0.55
5c	393.33	6	1	2	71.75	4.45	-6.87	High	Yes	0.55
5d	354.47	7	2	2	80.98	3.32	-5.79	High	No	0.55
5e	352.50	6	1	2	71.75	4.01	-5.73	High	Yes	0.55
5f	324.44	6	1	2	71.75	3.38	-5.68	High	Yes	0.55
5g	338.47	6	1	2	71.75	3.72	-6.06	High	Yes	0.55
5h	354.47	7	2	2	80.98	3.38	-5.79	High	No	0.55
5i	372.91	7	1	2	71.75	3.95	-6.67	High	Yes	0.55
5j	369.44	7	3	2	117.57	2.98	-5.51	High	No	0.55
5k	361.50	8	3	2	84.22	1.99	-4.14	High	No	0.55
5l	352.50	8	1	2	71.75	3.70	-6.48	High	Yes	0.55
5m	403.34	6	1	2	71.75	4.02	-6.48	High	Yes	0.55
5n	403.34	6	1	2	111.66	4.01	-6.48	High	Yes	0.55
5o	369.44	7	3	2	117.57	2.98	-5.51	High	No	0.55
5p	338.47	7	1	2	71.75	3.42	-6.08	High	Yes	0.55
5q	342.43	6	2	2	71.75	3.73	-7.59	High	Yes	0.55
5r	352.50	7	1	2	71.75	3.74	-6.46	High	Yes	0.55

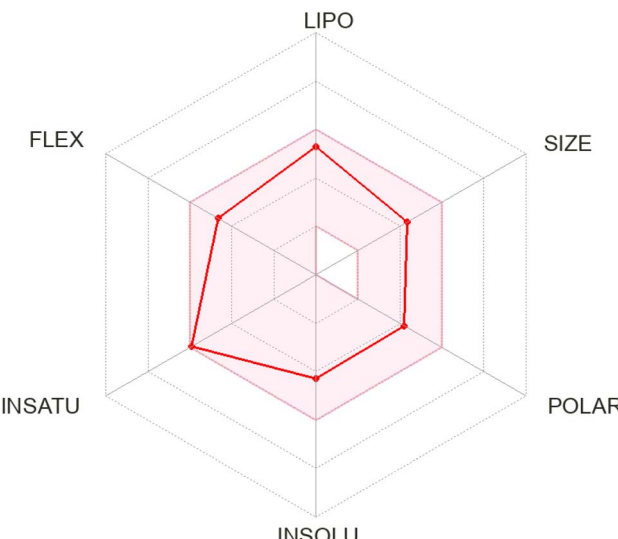


Fig. 7 Bioavailability radar diagram for compound 5d showing favorable oral bioavailability profile.

(1 H, s), 10.02 (1 H, s), 8.05 (1 H, s), 7.84 (1 H, d, *J* 8.0), 7.64 (2 H, d, *J* 8.3), 7.54 (1 H, d, *J* 8.1), 7.39 (1 H, t, *J* 8.1), 6.56 (2 H, d, *J* 8.4), 3.29 (4 H, d, *J* 6.4), 2.01–1.90 (4 H, m); <sup>13</sup>C NMR (151 MHz, DMSO)  $\delta$  175.64, 149.52, 145.07, 139.17, 132.00, 129.59, 129.12, 128.22, 128.12, 127.96, 120.73, 111.98, 47.72, 25.43, HPLC: CH<sub>3</sub>CN : H<sub>2</sub>O = 80 : 20; *tR*: 3.956 min, purity: 98.3%, C<sub>18</sub>H<sub>18</sub>Cl<sub>2</sub>N<sub>4</sub>S, QTOF MS ES<sup>+</sup> (*m/z*): [M + H]<sup>+</sup>, calcd: 393.0707, found: 393.0706.

**3.3.4 *N*-(4-Methoxyphenyl)-2-[4-(pyrrolidin-1-yl)benzylidene]hydrazinecarbothioamide (5d).** Color: light yellow, yield: 87%, melting point: 232–234 °C,  $\delta$ <sub>H</sub> (600 MHz, DMSO-*d*<sub>6</sub>) 11.49 (1 H, s), 9.80 (1 H, s), 8.03 (1 H, s), 7.67 (2 H, d, *J* 8.3), 7.43 (2 H, d, *J* 8.4), 6.92 (2 H, d, *J* 8.5), 6.55 (2 H, d, *J* 8.4), 3.77 (3 H, s), 3.28 (4 H, d, *J* 6.4), 2.03–1.85 (4 H, m); <sup>13</sup>C NMR (151 MHz, DMSO)  $\delta$  175.70, 157.20, 149.34, 144.40, 132.62, 129.59, 127.74,

121.07, 113.64, 111.88, 55.69, 47.71, 25.43, HPLC: CH<sub>3</sub>CN : H<sub>2</sub>O = 80 : 20; *tR*: 1.977 min, purity: 98.3%, C<sub>19</sub>H<sub>22</sub>N<sub>4</sub>OS, QTOF MS ES<sup>+</sup> (*m/z*): [M + H]<sup>+</sup>, calcd: 355.1592, found: 355.1582.

**3.3.5 *N*-(2,6-Dimethylphenyl)-2-[4-(pyrrolidin-1-yl)benzylidene]hydrazinecarbothioamide (5e).** Color: yellow, yield: 85%, melting point: 218–220 °C,  $\delta$ <sub>H</sub> (600 MHz, DMSO-*d*<sub>6</sub>) 11.46 (1 H, s), 9.64 (1 H, s), 8.01 (1 H, s), 7.68 (2 H, d, *J* 8.4), 7.11 (3 H, q, *J* 5.1), 6.54 (2 H, d, *J* 8.4), 3.29 (4 H, d, *J* 6.4), 2.20 (6 H, s), 2.02–1.91 (4 H, m); <sup>13</sup>C NMR (151 MHz, DMSO)  $\delta$  176.37, 149.25, 143.92, 137.89, 137.01, 129.50, 127.97, 127.18, 121.34, 111.86, 47.72, 25.43, 18.63, HPLC: CH<sub>3</sub>CN : H<sub>2</sub>O = 80 : 20; *tR*: 2.300 min, purity: 97.9%, C<sub>20</sub>H<sub>24</sub>N<sub>4</sub>S, QTOF MS ES<sup>+</sup> (*m/z*): [M + H]<sup>+</sup>, calcd: 353.1799, found: 353.1789.

**3.3.6 *N*-Phenyl-2-[4-(pyrrolidin-1-yl)benzylidene]hydrazinecarbothioamide (5f).** Color: yellow, yield: 83%, melting point: 270–272 °C,  $\delta$ <sub>H</sub> (600 MHz, DMSO-*d*<sub>6</sub>) 11.58 (1 H, s), 9.91 (1 H, s), 8.04 (1 H, s), 7.75–7.63 (2 H, m), 7.66–7.56 (2 H, m), 7.36 (2 H, t, *J* 7.9), 7.19 (1 H, dd, *J* 8.1, 6.6), 6.55 (2 H, d, *J* 8.6), 3.33–3.24 (4 H, m), 2.00–1.91 (4 H, m); <sup>13</sup>C NMR (151 MHz, DMSO)  $\delta$  175.23, 149.41, 144.69, 139.71, 129.66, 128.45, 125.88, 125.41, 120.95, 111.89, 47.72, 25.43, HPLC: CH<sub>3</sub>CN : H<sub>2</sub>O = 80 : 20; *tR*: 2.150 min, purity: 97.5%, C<sub>18</sub>H<sub>20</sub>N<sub>4</sub>S, QTOF MS ES<sup>+</sup> (*m/z*): [M + H]<sup>+</sup>, calcd: 325.1486, found: 325.1463.

**3.3.7 2-[4-(Pyrrolidin-1-yl)benzylidene]-*N*-(*p*-tolyl)hydrazinecarbothioamide (5g).** Color: yellow, yield: 81%, melting point: 230–232 °C,  $\delta$ <sub>H</sub> (600 MHz, DMSO-*d*<sub>6</sub>) 11.53 (1 H, s), 9.83 (1 H, s), 8.03 (1 H, s), 7.68 (2 H, d, *J* 8.7), 7.52–7.42 (2 H, m), 7.16 (2 H, d, *J* 8.1), 6.55 (2 H, d, *J* 8.7), 3.32–3.23 (4 H, m), 2.31 (3 H, s), 2.01–1.91 (4 H, m); <sup>13</sup>C NMR (151 MHz, DMSO)  $\delta$  175.32, 149.37, 144.53, 137.14, 134.54, 129.62, 128.92, 125.88, 121.00, 111.89, 47.71, 25.43, 21.06, HPLC: CH<sub>3</sub>CN : H<sub>2</sub>O = 80 : 20; *tR*: 2.459 min, purity: 97.7%, C<sub>19</sub>H<sub>22</sub>N<sub>4</sub>S, QTOF MS ES<sup>+</sup> (*m/z*): [M + H]<sup>+</sup>, calcd: 339.1643, found: 339.1630.

**3.3.8 *N*-(3-Methoxyphenyl)-2-[4-(pyrrolidin-1-yl)benzylidene]hydrazinecarbothioamide (5h).** Color: shine yellow, yield: 95%, melting point: 220–222 °C,  $\delta$ <sub>H</sub> (600 MHz,



DMSO-*d*<sub>6</sub>) 11.60 (1 H, s), 9.86 (1 H, s), 8.04 (1 H, s), 7.74–7.64 (2 H, m), 7.36 (1 H, t, *J* 2.1), 7.30–7.19 (2 H, m), 6.76 (1 H, dt, *J* 7.5, 2.1), 6.60–6.50 (2 H, m), 3.77 (3 H, s), 3.28 (4 H, q, *J* 4.7, 3.2), 2.01–1.91 (4 H, m); <sup>13</sup>C NMR (151 MHz, DMSO)  $\delta$  174.90, 159.44, 149.43, 144.77, 140.81, 129.69, 129.14, 120.88, 117.71, 112.09, 111.90, 111.17, 110.83, 55.60, 47.71, 25.43, HPLC: CH<sub>3</sub>CN : H<sub>2</sub>O = 80 : 20; *t*R: 2.166 min, purity: 97.1%, C<sub>19</sub>H<sub>22</sub>N<sub>4</sub>OS, QTOF MS ES+ (*m/z*): [M + H]<sup>+</sup>, calcd: 355.1592, found: 355.1582.

### 3.3.9 *N*-(4-Chlorobenzyl)-2-[4-(pyrrolidin-1-yl)benzylidene]hydrazinecarbothioamide (5i).

Color: brown, yield: 79%, melting point: 234–236 °C,  $\delta$ <sub>H</sub> (600 MHz, DMSO-*d*<sub>6</sub>) 11.36 (1 H, s), 8.89 (1 H, t, *J* 6.3), 7.97 (1 H, s), 7.59 (2 H, d, *J* 8.6), 7.38 (4 H, s), 6.53 (2 H, dd, *J* 8.6, 2.0), 4.81 (2 H, d, *J* 6.3), 3.32–3.22 (4 H, m), 1.99–1.92 (4 H, m); <sup>13</sup>C NMR (151 MHz, DMSO)  $\delta$  177.21, 149.26, 144.13, 139.30, 131.64, 129.62, 129.56, 129.30, 129.07, 128.54, 121.15, 111.87, 47.70, 46.27, 25.42, HPLC: CH<sub>3</sub>CN : H<sub>2</sub>O = 80 : 20; *t*R: 2.558 min, purity: 96.3%, C<sub>19</sub>H<sub>21</sub>ClN<sub>4</sub>S, QTOF MS ES+ (*m/z*): [M + H]<sup>+</sup>, calcd: 373.1253, found: 373.1253.

### 3.3.10 *N*-(4-Nitrophenyl)-2-[4-(pyrrolidin-1-yl)benzylidene]hydrazinecarbothioamide (5j).

Color: orange, yield: 85%, melting point: 250–252 °C,  $\delta$ <sub>H</sub> (600 MHz, DMSO-*d*<sub>6</sub>) 11.95 (1 H, s), 10.28 (1 H, s), 8.26–8.21 (2 H, m), 8.15–8.10 (2 H, m), 8.08 (1 H, s), 7.72–7.67 (2 H, m), 6.61–6.52 (2 H, m), 3.32–3.25 (4 H, m), 2.00–1.93 (4 H, m); <sup>13</sup>C NMR (151 MHz, DMSO)  $\delta$  174.30, 149.62, 146.12, 145.93, 143.53, 129.95, 124.21, 124.19, 120.52, 111.91, 47.72, 25.42, HPLC: CH<sub>3</sub>CN : H<sub>2</sub>O = 80 : 20; *t*R: 2.344 min, purity: 98.8%, C<sub>18</sub>H<sub>19</sub>N<sub>5</sub>O<sub>2</sub>S, QTOF MS ES+ (*m/z*): [M + H]<sup>+</sup>, calcd: 370.1337, found: 370.1337.

### 3.3.11 *N*-(2-Morpholinoethyl)-2-[4-(pyrrolidin-1-yl)benzylidene]hydrazinecarbothioamide (5k).

Color: off-white, yield: 89%, melting point: 227–229 °C,  $\delta$ <sub>H</sub> (600 MHz, DMSO-*d*<sub>6</sub>) 11.25 (1 H, s), 8.26 (1 H, t, *J* 5.5), 7.93 (1 H, s), 7.60–7.51 (2 H, m), 6.62–6.51 (2 H, m), 3.65 (2 H, q, *J* 6.4), 3.60 (4 H, t, *J* 4.6), 3.32–3.25 (4 H, m), 2.53 (2 H, t, *J* 6.7), 2.44 (4 H, s), 2.00–1.92 (4 H, m); <sup>13</sup>C NMR (151 MHz, DMSO)  $\delta$  176.54, 149.28, 143.67, 129.02, 121.13, 111.95, 66.83, 57.09, 53.65, 47.72, 25.43, HPLC: CH<sub>3</sub>CN : H<sub>2</sub>O = 80 : 20; *t*R: 1.610 min, purity: 98.9%, C<sub>18</sub>H<sub>27</sub>N<sub>5</sub>OS, QTOF MS ES+ (*m/z*): [M + H]<sup>+</sup>, calcd: 362.2014, found: 362.2014.

### 3.3.12 *N*-Phenethyl-2-[4-(pyrrolidin-1-yl)benzylidene]hydrazinecarbothioamide (5l).

Color: off-white, yield: 91%, melting point: 237–239 °C,  $\delta$ <sub>H</sub> (600 MHz, DMSO-*d*<sub>6</sub>) 11.25 (1 H, s), 8.31 (1 H, t, *J* 5.9), 7.93 (1 H, s), 7.60–7.52 (2 H, m), 7.33 (2 H, t, *J* 7.5), 7.31–7.26 (2 H, m), 7.26–7.21 (1 H, m), 6.58–6.52 (2 H, m), 3.76 (2 H, ddd, *J* 9.4, 7.7, 5.9), 3.33–3.23 (4 H, m), 2.96–2.87 (2 H, m), 2.01–1.90 (4 H, m); <sup>13</sup>C NMR (151 MHz, DMSO)  $\delta$  176.61, 149.26, 143.73, 139.82, 129.15, 129.09, 128.94, 126.66, 121.17, 111.91, 47.72, 45.37, 35.51, 25.43, HPLC: CH<sub>3</sub>CN : H<sub>2</sub>O = 80 : 20; *t*R: 2.608 min, purity: 98.4%, C<sub>20</sub>H<sub>24</sub>N<sub>4</sub>S, QTOF MS ES+ (*m/z*): [M + H]<sup>+</sup>, calcd: 353.1799, found: 353.1799.

### 3.3.13 *N*-(4-Bromophenyl)-2-[4-(pyrrolidin-1-yl)benzylidene]hydrazinecarbothioamide (5m).

Color: off-white, yield: 91%, melting point: 228–230 °C,  $\delta$ <sub>H</sub> (600 MHz, DMSO-*d*<sub>6</sub>) 11.67 (1 H, s), 9.95 (1 H, s), 8.04 (1 H, s), 7.70–7.66 (2 H, m), 7.64–7.59 (2 H, m), 7.56–7.51 (2 H, m), 6.61–6.51 (2 H, m), 3.32–3.25 (4 H, m), 1.99–1.92 (4 H, m); <sup>13</sup>C NMR (151 MHz, DMSO)  $\delta$  175.07, 149.46, 145.04, 139.15, 131.23, 129.73, 127.80, 120.84,

117.55, 111.89, 47.72, 25.43, HPLC: CH<sub>3</sub>CN : H<sub>2</sub>O = 80 : 20; *t*R: 3.025 min, purity: 97.4%, C<sub>18</sub>H<sub>19</sub>BrN<sub>4</sub>S, QTOF MS ES+ (*m/z*): [M + H]<sup>+</sup>, calcd: 403.0592, found: 403.0503.

### 3.3.14 *N*-(3-Bromophenyl)-2-[4-(pyrrolidin-1-yl)benzylidene]hydrazinecarbothioamide (5n).

Color: green, yield: 85%, melting point: 223–225 °C,  $\delta$ <sub>H</sub> (600 MHz, DMSO-*d*<sub>6</sub>) 11.71 (1 H, s), 8.05 (1 H, s), 7.95 (1 H, t, *J* 2.0), 7.75–7.66 (3 H, m), 7.36 (1 H, dt, *J* 8.0, 1.4), 7.32 (1 H, t, *J* 8.0), 6.60–6.52 (2 H, m), 3.34–3.24 (4 H, m), 2.01–1.90 (4 H, m); <sup>13</sup>C NMR (151 MHz, DMSO)  $\delta$  174.93, 149.48, 145.18, 141.36, 130.25, 129.78, 127.94, 127.88, 124.58, 120.91, 120.79, 112.06, 111.88, 47.72, 25.43, HPLC: CH<sub>3</sub>CN : H<sub>2</sub>O = 80 : 20; *t*R: 3.022 min, purity: 97.2%, C<sub>18</sub>H<sub>19</sub>BrN<sub>4</sub>S, QTOF MS ES+ (*m/z*): [M + H]<sup>+</sup>, calcd: 403.0592, found: 403.0522.

### 3.3.15 *N*-(3-Nitrophenyl)-2-[4-(pyrrolidin-1-yl)benzylidene]hydrazinecarbothioamide (5o).

Color: yellow, yield: 85%, melting point: 220–222 °C,  $\delta$ <sub>H</sub> (600 MHz, DMSO-*d*<sub>6</sub>) 11.85 (1 H, s), 10.24 (1 H, s), 8.71 (1 H, t, *J* 2.2), 8.21–8.13 (1 H, m), 8.07 (1 H, s), 8.02 (1 H, ddd, *J* 8.2, 2.4, 1.0), 7.77–7.66 (2 H, m), 7.64 (1 H, t, *J* 8.1), 6.62–6.51 (2 H, m), 3.33–3.25 (4 H, m), 2.00–1.92 (4 H, m); <sup>13</sup>C NMR (151 MHz, DMSO)  $\delta$  174.96, 149.55, 147.69, 145.63, 140.99, 131.83, 129.86, 129.56, 120.68, 119.71, 119.69, 111.89, 47.72, 25.43, HPLC: CH<sub>3</sub>CN : H<sub>2</sub>O = 80 : 20; *t*R: 2.207 min, purity: 97.9%, C<sub>18</sub>H<sub>19</sub>N<sub>5</sub>O<sub>2</sub>S, QTOF MS ES+ (*m/z*): [M + H]<sup>+</sup>, calcd: 370.1337, found: 370.1337.

### 3.3.16 *N*-Benzyl-2-[4-(pyrrolidin-1-yl)benzylidene]hydrazinecarbothioamide (5p).

Color: off-white, yield: 85%, melting point: 181–183 °C,  $\delta$ <sub>H</sub> (600 MHz, DMSO-*d*<sub>6</sub>) 11.33 (1 H, s), 8.85 (1 H, t, *J* 6.3), 7.97 (1 H, s), 7.64–7.55 (2 H, m), 7.38–7.35 (2 H, m), 7.35–7.30 (2 H, m), 7.27–7.20 (1 H, m), 6.58–6.48 (2 H, m), 4.84 (2 H, d, *J* 6.3), 3.32–3.22 (4 H, m), 2.02–1.90 (4 H, m); <sup>13</sup>C NMR (151 MHz, DMSO)  $\delta$  177.19, 149.25, 144.00, 140.21, 129.27, 128.60, 127.73, 127.13, 121.19, 111.88, 47.70, 46.93, 25.42, HPLC: CH<sub>3</sub>CN : H<sub>2</sub>O = 80 : 20; *t*R: 2.202 min, purity: 98.1%, C<sub>19</sub>H<sub>22</sub>N<sub>4</sub>S, QTOF MS ES+ (*m/z*): [M + H]<sup>+</sup>, calcd: 339.1643, found: 339.1643.

### 3.3.17 *N*-(2-Fluorophenyl)-2-[4-(pyrrolidin-1-yl)benzylidene]hydrazinecarbothioamide (5q).

Color: green, yield: 87%, melting point: 228–230 °C,  $\delta$ <sub>H</sub> (600 MHz, DMSO-*d*<sub>6</sub>) 11.60 (1 H, s), 9.92 (1 H, s), 8.03 (1 H, s), 7.74–7.64 (2 H, m), 7.65–7.53 (2 H, m), 7.26–7.13 (2 H, m), 6.62–6.51 (2 H, m), 3.28 (4 H, d, *J* 6.3), 2.00–1.91 (4 H, m); <sup>13</sup>C NMR (151 MHz, DMSO)  $\delta$  175.61, 160.73, 159.13, 149.41, 144.77, 136.09, 136.07, 129.67, 128.27, 128.21, 120.95, 115.13, 114.98, 111.88, 47.71, 25.43, HPLC: CH<sub>3</sub>CN : H<sub>2</sub>O = 80 : 20; *t*R: 2.164 min, purity: 98.6%, C<sub>18</sub>H<sub>19</sub>FN<sub>4</sub>S, QTOF MS ES+ (*m/z*): [M + H]<sup>+</sup>, calcd: 343.1392, found: 343.1395.

### 3.3.18 *N*-(4-Methylbenzyl)-2-[4-(pyrrolidin-1-yl)benzylidene]hydrazinecarbothioamide (5r).

Color: off-white, yield: 87%, melting point: 205–207 °C,  $\delta$ <sub>H</sub> (600 MHz, DMSO-*d*<sub>6</sub>) 11.30 (1 H, s), 8.78 (1 H, t, *J* 6.3), 7.96 (1 H, s), 7.63–7.53 (2 H, m), 7.32–7.21 (2 H, m), 7.13 (2 H, d, *J* 7.8), 6.59–6.47 (2 H, m), 4.79 (2 H, d, *J* 6.2), 3.30–3.20 (4 H, m), 2.28 (3 H, s), 2.00–1.89 (4 H, m); <sup>13</sup>C NMR (151 MHz, DMSO)  $\delta$  177.08, 149.24, 143.94, 137.12, 136.15, 129.25, 129.14, 127.77, 121.20, 111.88, 47.70, 46.70, 25.42, 21.18, HPLC: CH<sub>3</sub>CN : H<sub>2</sub>O = 80 : 20; *t*R: 2.603 min,



purity: 98.3%,  $C_{20}H_{24}N_4S$ , QTOF MS ES<sup>+</sup> ( $m/z$ ):  $[M + H]^+$ , calcd: 353.1799, found: 353.1799.

## 4. Conclusion

In conclusion, the comprehensive study into the potential of 4-pyrrolidine-based thiosemicarbazones **5(a–r)** as DHFR inhibitors through *in vitro* and *in silico* studies sheds light on their promising therapeutic applications. The synthesized compounds **5(a–r)** demonstrated notable inhibitory activity against DHFR with  $IC_{50}$  value in the range of  $12.37 \pm 0.48 \mu\text{M}$  to  $54.10 \pm 0.72 \mu\text{M}$ , showcasing their potential as effective agents against various diseases, including cancer and microbial infections. Amongst all derivatives, **5d** is more potent towards DHFR enzyme. Furthermore, the molecular docking simulations provided valuable insights into the binding interactions between the compounds **5(a–r)** and the target enzyme, elucidating their mechanism of action at the molecular level. These findings underscore the significance of further exploration and optimization of 4-pyrrolidine-based thiosemicarbazones for the development of novel DHFR inhibitors with enhanced efficacy and reduced toxicity, thereby offering new avenues for drug discovery and therapeutic invention.

## Data availability

The data supporting this article have been included as part of the ESI.†

## Conflicts of interest

The authors have declared no conflict of interest.

## Acknowledgements

Authors are thankful to the Researchers Supporting Project number (RSP2024R491), King Saud University, Riyadh, Saudi Arabia. Z. S. is thankful to the Alexander von Humboldt Foundation for the award of the Georg Forster Research Fellowship for Experienced Researchers.

## References

- 1 A. Aggarwal, O. Ginsburg and T. Fojo, Cancer economics, policy and politics: what informs the debate? Perspectives from the EU, Canada and US, *J. Cancer Policy*, 2014, **2**(1), 1–11.
- 2 P. Singh, M. Kaur and S. Sachdeva, Mechanism inspired development of rationally designed dihydrofolate reductase inhibitors as anticancer agents, *J. Med. Chem.*, 2012, **55**(14), 6381–6390.
- 3 A. Wróbel, M. Baradyn, A. Ratkiewicz and D. Drozdowska, Synthesis, biological activity, and molecular dynamics study of novel series of a trimethoprim analogs as multi-targeted compounds: Dihydrofolate reductase (DHFR) inhibitors and DNA-binding agents, *Int. J. Mol. Sci.*, 2021, **22**(7), 3685.
- 4 C. Capasso and C. T. Supuran, Sulfa and trimethoprim-like drugs–antimetabolites acting as carbonic anhydrase, dihydropteroate synthase and dihydrofolate reductase inhibitors, *J. Enzyme Inhib. Med. Chem.*, 2014, **29**(3), 379–387.
- 5 A. Rao and S. Tapale, A study on dihydrofolate reductase and its inhibitors: A review, *Int. J. Pharm. Sci. Res.*, 2013, **4**(7), 2535.
- 6 E. O. Osman, S. H. Emam, A. Sonousi, M. M. Kandil, A. M. Abdou and R. A. Hassan, Design, synthesis, anticancer, and antibacterial evaluation of some quinazolinone-based derivatives as DHFR inhibitors, *Drug Dev. Res.*, 2023, **84**(5), 888–906.
- 7 G. Tcherkez, E. Boex-Fontvieille, A. Mahé and M. Hodges, Respiratory carbon fluxes in leaves, *Curr. Opin. Plant Biol.*, 2012, **15**(3), 308–314.
- 8 M. V. Raimondi, O. Randazzo, M. La Franca, G. Barone, E. Vignoni, D. Rossi and S. Collina, DHFR inhibitors: reading the past for discovering novel anticancer agents, *Molecules*, 2019, **24**(6), 1140.
- 9 H. Li, F. Fang, Y. Liu, L. Xue, M. Wang, Y. Guo, X. Wang, C. Tian, J. Liu and Z. Zhang, Inhibitors of dihydrofolate reductase as antitumor agents: design, synthesis and biological evaluation of a series of novel nonclassical 6-substituted pyrido [3, 2-d] pyrimidines with a three-to five-carbon bridge, *Bioorg. Med. Chem.*, 2018, **26**(9), 2674–2685.
- 10 W. D. Alrohily, M. E. Habib, S. M. El-Messery, A. Alqurshy, H. El-Subbagh and E.-S. E. Habib, Antibacterial, antibiofilm and molecular modeling study of some antitumor thiazole based chalcones as a new class of DHFR inhibitors, *Microb. Pathog.*, 2019, **136**, 103674.
- 11 Y.-C. Hsieh, N. E. Skacel, N. Bansal, K. W. Scotto, D. Banerjee, J. R. Bertino and E. E. Abali, Species-specific differences in translational regulation of dihydrofolate reductase, *Mol. Pharmacol.*, 2009, **76**(4), 723–733.
- 12 G. Li Petri, M. V. Raimondi, V. Spanò, R. Holl, P. Barraja and A. Montalbano, Pyrrolidine in drug discovery: a versatile scaffold for novel biologically active compounds, *Top. Curr. Chem.*, 2021, **379**, 1–46.
- 13 A. A. Bhat, I. Singh, N. Tandon and R. Tandon, Structure activity relationship (SAR) and anticancer activity of pyrrolidine derivatives: Recent developments and future prospects (A review), *Eur. J. Med. Chem.*, 2023, **246**, 114954.
- 14 M. Tasleem, J. Pelletier, J. Sévigny, Z. Hussain, A. Khan, A. Al-Harrasi, A. F. El-Kott, P. Taslimi, S. Negm, Z. Shafiq and J. Iqbal, Synthesis, *in vitro*, and *in silico* studies of morpholine-based thiosemicarbazones as ectonucleotide pyrophosphatase/phosphodiesterase-1 and-3 inhibitors, *Int. J. Biol. Macromol.*, 2024, **266**, 131068.
- 15 A. Gomtsyan, Heterocycles in drugs and drug discovery, *Chem. Heterocycl. Compd.*, 2012, **48**, 7–10.
- 16 A. Hamad, M. A. Khan, K. M. Rahman, I. Ahmad, Z. Ul-Haq, S. Khan and Z. Shafiq, Development of sulfonamide-based Schiff bases targeting urease inhibition: Synthesis, characterization, inhibitory activity assessment, molecular docking and ADME studies, *Bioorg. Chem.*, 2020, **102**, 104057.



- 17 M. T. Shehzad, A. Khan, M. Islam, A. Hameed, M. Khiat, S. A. Halim, M. U. Anwar, S. R. Shah, J. Hussain and R. Csuk, Synthesis and urease inhibitory activity of 1, 4-benzodioxane-based thiosemicarbazones: Biochemical and computational approach, *J. Mol. Struct.*, 2020, **1209**, 127922.
- 18 M. Arooj, M. Zahra, M. Islam, N. Ahmed, A. Waseem and Z. Shafiq, Coumarin based thiosemicarbazones as effective chemosensors for fluoride ion detection, *Spectrochim. Acta, Part A*, 2021, **261**, 120011.
- 19 M. D. Altintop, Z. A. Kaplancıklı, G. A. Çiftçi and R. Demirel, Synthesis and biological evaluation of thiazoline derivatives as new antimicrobial and anticancer agents, *Eur. J. Med. Chem.*, 2014, **74**, 264–277.
- 20 Y. Qin, R. Xing, S. Liu, K. Li, X. Meng, R. Li, J. Cui, B. Li and P. Li, Novel thiosemicarbazone chitosan derivatives: Preparation, characterization, and antifungal activity, *Carbohydr. Polym.*, 2012, **87**(4), 2664–2670.
- 21 A. Pyrih, M. Jaskolski, A. K. Gzella and R. Lesyk, Synthesis, structure and evaluation of anticancer activity of 4-amino-1, 3-thiazolinone/pyrazoline hybrids, *J. Mol. Struct.*, 2021, **1224**, 129059.
- 22 J. F. Machado, F. Marques, T. Pinheiro, M. J. Villa de Brito, G. Scalese, L. Pérez-Díaz, L. Otero, J. P. António, D. Gambino and T. S. Morais, Copper (I)-Thiosemicarbazone Complexes with Dual Anticancer and Antiparasitic Activity, *ChemMedChem*, 2023, **18**(14), e202300074.
- 23 M. Scaccaglia, S. Pinelli, L. Manini, B. Ghezzi, M. Nicastro, J. Heinrich, N. Kulak, P. Mozzoni, G. Pelosi and F. Bisceglie, Gold (III) complexes with thiosemicarbazone ligands: insights into their cytotoxic effects on lung cancer cells, *J. Inorg. Biochem.*, 2024, **251**, 112438.
- 24 M. T. Shehzad, A. Hameed, M. Al-Rashida, A. Imran, M. Uroos, A. Asari, H. Mohamad, M. Islam, S. Iftikhar and Z. Shafiq, Exploring antidiabetic potential of adamantyl-thiosemicarbazones via aldose reductase (ALR2) inhibition, *Bioorg. Chem.*, 2019, **92**, 103244.
- 25 S. Umamatheswari, B. Balaji, M. Ramanathan and S. Kabilan, Synthesis, stereochemistry, antimicrobial evaluation and QSAR studies of 2, 6-diaryltetrahydropyran-4-one thiosemicarbazones, *Eur. J. Med. Chem.*, 2011, **46**(4), 1415–1424.
- 26 M. Ertas, Z. Sahin, E. F. Bulbul, C. Bender, S. N. Biltakin, B. Berk, L. Yurttas, A. M. Nalbur, H. Celik and S. Demirayak, Potent ribonucleotide reductase inhibitors: Thiazole-containing thiosemicarbazone derivatives, *Arch. Pharm.*, 2019, **352**(11), 1900033.
- 27 A. Imran, M. T. Shehzad, S. J. A. Shah, T. Al Adhami, M. Laws, K. M. Rahman, R. D. Alharthy, I. A. Khan, Z. Shafiq and J. Iqbal, Development and exploration of novel substituted thiosemicarbazones as inhibitors of aldose reductase via in vitro analysis and computational study, *Sci. Rep.*, 2022, **12**(1), 5734.
- 28 X. Jiang, L. A. Fielding, H. Davis, W. Carroll, E. C. Lisic and J. E. Deweese, Inhibition of topoisomerases by metal thiosemicarbazone complexes, *Int. J. Mol. Sci.*, 2023, **24**(15), 12010.
- 29 R. H. Dhabale, S. Shah, N. Tiwari and P. Patani, Review of Semicarbazone, Thiosemicarbazone, and their transition metal complexes, and their biological activities, *J. Pharm. Negat. Results*, 2022, 2416–2424.
- 30 D. S. Kalinowski, P. Quach and D. R. Richardson, Thiosemicarbazones: the new wave in cancer treatment, *Future Med. Chem.*, 2009, **1**(6), 1143–1151.
- 31 Y. Yu, D. S. Kalinowski, Z. Kovacevic, A. R. Siafakas, P. J. Jansson, C. Stefani, D. B. Lovejoy, P. C. Sharpe, P. V. Bernhardt and D. R. Richardson, Thiosemicarbazones from the old to new: iron chelators that are more than just ribonucleotide reductase inhibitors, *J. Med. Chem.*, 2009, **52**(17), 5271–5294.
- 32 N. Arumugam, A. I. Almansour, R. S. Kumar, V. S. Krishna, D. Sriram and N. Dege, Stereoselective synthesis and discovery of novel spirooxindolopyrrolidine engrafted indandione heterocyclic hybrids as antimycobacterial agents, *Bioorg. Chem.*, 2021, **110**, 104798.
- 33 A. Ragab, Y. A. Ammar, A. Ezzat, A. M. Mahmoud, M. B. I. Mohamed, S. Abdou and R. S. Farag, Synthesis, characterization, thermal properties, antimicrobial evaluation, ADMET study, and molecular docking simulation of new mono Cu (II) and Zn (II) complexes with 2-oxoindole derivatives, *Comput. Biol. Med.*, 2022, **145**, 105473.
- 34 N. W. Hassan, A. Sabt, M. A. El-Attar, M. Ora, A. E.-D. A. Bekhit, K. Amagase, A. A. Bekhit, A. S. Belal and P. A. Elzahhar, Modulating leishmanial pteridine metabolism machinery via some new coumarin-1, 2, 3-triazoles: Design, synthesis and computational studies, *Eur. J. Med. Chem.*, 2023, **253**, 115333.
- 35 G. S. Hassan, S. M. El-Messery, F. A. Al-Omary, S. T. Al-Rashood, M. I. Shabayek, Y. S. Abulfadl, E.-S. E. Habib, S. M. El-Hallouty, W. Fayad and K. M. Mohamed, Nonclassical antifolates, part 4. 5-(2-Aminothiazol-4-yl)-4-phenyl-4H-1, 2, 4-triazole-3-thiols as a new class of DHFR inhibitors: Synthesis, biological evaluation and molecular modeling study, *Eur. J. Med. Chem.*, 2013, **66**, 135–145.
- 36 M. B. Tufail, M. A. Javed, M. Ikram, M. H. Mahnashi, B. A. Alyami, Y. S. Alqahtani, A. Sadiq and U. Rashid, Synthesis, pharmacological evaluation and Molecular modelling studies of pregnenolone derivatives as inhibitors of human dihydrofolate reductase, *Steroids*, 2021, **168**, 108801.
- 37 R. A. Markandewar, H. M. Zia and M. Baseer, Impact of reaction dynamics on synthesis of novel nitrogen containing aldehydes, *Orient. J. Chem.*, 2013, **29**(4), 1531–1534.
- 38 D. Taşdemir, A. Karaküçük-İyidoğan, M. Ulaşlı, T. Taşkin-Tok, E. E. Oruç-Emre and H. Bayram, Synthesis, molecular modeling, and biological evaluation of novel chiral thiosemicarbazone derivatives as potent anticancer agents, *Chirality*, 2015, **27**(2), 177–188.

